Evolutionary Intelligence
https://doi.org/10.1007/s12065-021-00627-5

RESEARCH PAPER

Enhanced statistical nearest neighbors with steerable pyramid transform for Gaussian noise removal in a color image

Akula Suneetha[1] · **Edara Srinivasa Reddy**[2]

Received: 21 December 2020 / Revised: 17 March 2021 / Accepted: 29 May 2021
© The Author(s), under exclusive licence to Springer-Verlag GmbH Germany, part of Springer Nature 2021

Abstract
Image denoising is the foremost issue in the field of image processing and computer vision applications and the most challenging part in image denoising is to protect the data bearing structures like surfaces and edges to achieve better visual image quality. The non-local means filtering technique perform well to denoise Gaussian noise, while preserving the edges and details of the original images, In this paper, an effective Gaussian denoiser is proposed based on non-local means filter to improve the resulting image quality. An exponential kernel function is included in the statistical nearest neighbor to decrease the prediction error in noise free patches, which deblurs the lower contrast image details effectively. Further, steerable pyramid transform is applied along with hard thresholding to generate the image with better visible level. The simulation outcome showed that the proposed enhanced statistical nearest neighbors with steerable pyramid transform model achieved better Gaussian denoising performance in terms of feature similarity index, structural similarity index, mean structural similarity index, peak signal-to-noise ratio, and feature similarity index with chromatic information. In the experimental section, proposed model showed a maximum of 2.07 dB and minimum of 0.70 dB improvement in peak signal-to-noise ratio value compared to the existing model; non-local means- statistical nearest neighbor and attention-guided denoising convolutional neural network.

Keywords Color image denoising · Hard thresholding · Kernel function · Statistical nearest neighbor · Steerable pyramid transform

1 Introduction

In recent decades, image denoising is a major concern in image restoration and several image processing applications. The noise reduction is an important step to achieve accurate information from the sub-sequent processes like object detection, segmentation and classification [1–3]. In addition, image denoising makes a tradeoff between the feature preservation and noise removal. Currently, color images are widely applied in several applications, which are corrupted by the noises because of its image collection mechanism, storage or transmission [4, 5]. Usually, impulse noise, Gaussian noise, and mixed noise are the common types of noises occurred in the collected color images [6, 7]. Multi-level edge features guided network [8], multi-scale dilated residual network [9], adaptive weighted TVp regularization [10], non-local self-similarity [11], fractional derivatives [12], deep orthogonal transform feature [13], etc. are some of the techniques developed by the researchers to avoid the damage of clean pixels in the color images to improve image denoising performance. In specific, directional distance filter, vector median filter and vector directional filter are the most common non-linear filters used in Gaussian noise removal, where these existing non-linear filters are spatially invariant which makes no distinctions between the noise free and noisy image pixels. Unlike local means filter, a Non Local Means (NLM) filter operates on non-local area utilizing a dissimilarity measure between the image patches, where the NLM filter works well in eliminating Gaussian noise.

✉ Akula Suneetha
sunitha.akula1.cse@gmail.com; sunitha_akula1@yahoo.co.in

Edara Srinivasa Reddy
edara_67@yahoo.com

[1] Department of CSE, KKR and KSR Institute of Technology and Sciences, Guntur, Andhra Pradesh, India

[2] Department of CSE, University College of Engineering & Technology, Acharya Nagarjuna University, Nagarjuna Nagar, Guntur, Andhra Pradesh, India

Published online: 06 June 2021

Several research works based on NLM filter are developed to tradeoff the image detail preservation against noise reduction, where a few previous research works are surveyed in the literature section. By the reference Frosio, and Kautz, [22], Enhanced Statistical Nearest Neighbor (ESNN) is proposed with Steerable Pyramid Transform (SPT) in this research study for denoising the images under the circumstance of Gaussian noise. In ESNN, an approximate kernel function is included in SNN, which adjusts the local structure of image to improve the performance of image denoising. Additionally, SPT along with hard thresholding adjusts the local direction and anisotropic patterns that preserves and smooths the image edge details effectively. The extensive experiment showed that the proposed ESNN-SPT model attained better denoising performance by means of Feature Similarity Index (FSIM), Structural Similarity Index (SSIM), Mean Structural Similarity Index (MSSIM), Peak Signal-to-Noise Ratio (PSNR) and Feature Similarity Index with Chromatic information ($FSIM_c$). For experimental analysis, KODAK database (25 uncompressed images) is utilized in this study. This research article is prepared as follows. A few recent research papers on the topic "image denoising" is surveyed in the Sect. 2. The proposed ESNN-SPT model is explained in Sect. 3. The experimental evaluation of the proposed ESNN-SPT model is given in the Sect. 4. The conclusion of the present research work is given in the Sect. 5.

2 Literature review

Elhoseny and Shankar [14] developed a bio inspired optimization based filtering system for image denoising on the basis of the bilateral filter. The denoising process was influenced by selecting the optimal parameters like spatial and Gaussian weights. In this literature study, these parameters were selected using modified firefly and dragonfly optimization algorithms. At last, Convolutional Neural Network (CNN) was utilized for classifying the denoised images as normal or abnormal. The simulation outcome showed that the developed system achieved better denoising performance compared to the existing filters and classifiers in light of error value and PSNR value. However, the developed bio inspired optimization based filtering system have the issue of sparse matrices where it consumes more memory and time for denoising the images. Kumar et al. [15] used the concept of overlapping group sparsity for image denoising that was formulated by convex and non-convex denoising systems. The experimental results showed that the developed method attained better denoising performance than the existing methods irrespective of the image type and noise level. Here, it is essential to solve a minimization concern in the developed method which is computationally challenging.

Zha et al. [16] developed Group Sparsity Residual Constraint with External Nonlocal Self Similarity (GSRC-ENSS) model for image denoising. The conventional NSS based denoising approach exploits only NSS prior of natural or noisy images, but the developed ENSS exploits two priors (NSS priors of natural and noisy images) for image denoising. To further enhance the image denoising performance, GSR concept was used in this literature. The group sparse coefficients of the noisy images were exploited to approximate the estimation and the sparse coefficients of the natural images were exploited on the basis of Gaussian Mixture Model (GMM) learning. Finally, the iterative shrinkage algorithm was used to incorporate the NSS priors of noisy and natural images. The simulation result showed that the developed GSRC-ENSS model outperforms the existing models and delivers better qualitative denoising results with finer image details and less ringing noise. A major concern in sparse coding based model was to train a dictionary from natural and noisy images, which was a time consuming task. Fan et al. [17] implemented an adaptive boosting technique to enhance the lower-rank based image denoising. In this literature, the strength of the image signal was considered by leveraging the availability of the prior denoised image instead of adding the residual back to the image. Here, the developed boosting technique was combined with weighted nuclear norm minimization approach to gain an effective index of same image patches. Additionally, correlation coefficient was employed to find the optimal number of iteration for stopping criteria. The simulation results showed that the developed model preserves more detail information, while removing noise and also outperforms various existing denoising algorithms in light of PSNR and SSIM. Still, the developed model has limitations in some aspects; lack of consideration in the noise effects during the selection of same image patches and also highly reliance on empirical values, while setting the parameters.

Wang et al. [18] developed an Improved Non Local Means (INLM) filter for color image denoising that combines the benefits of bilateral filter and NLM filter. The developed INLM filter effectively eliminates the impulse noise, Gaussian noise and the mixture of impulse and Gaussian noise that were added to the original digital images. Further, the developed INLM filter preserves the image details well at dissimilar noise ratios. The experimental outcome showed that the developed INLM filter achieved better performance in reducing the noises in light of PSNR, MSE, and SSIM. The developed INLM filter effectively removes the noises, but still blocking artifacts and blurring exists in the images, which are considered as the major concerns in this literature

study. Li and Suen [19] introduced Grey theory based NLM (GNLM) technique for color image denoising. The grey theory was effective in handling the complex scenes and also requires few testing samples for achieving better denoising performance. The weight estimator in grey theory extracts the most significant image patch pairs for denoising. The developed GNLM technique solves the parameter setting issue, which encountered in NLM technique that diminishes the computational complexity. The experimental outcome showed that the developed GNLM technique effectively eliminates the noises and captures the image details; corner and edge. However, the developed GNLM technique has the problem of compact support and filter parameter selection.

Chen et al. [20] developed Collaborative Non Local Means (CNLM) filtering technique to denoise the images. In this literature, an NLM like block matching was carried-out on the aligned images with the target image as the reference to denoise the target and multiple images which were acquired from the different subjects. The developed CNLM technique significantly upsurges the matching structures that helps in boosting the denoising performance. The experiment results on both real and synthetic data showed that the developed CNLM technique outperforms the conventional NLM techniques by means of PSNR. The developed CNLM filtering technique blurs the medical image edges that was considered as one of the main issue, and also it estimates only grey level values which was not robust to attain better denoising performance. Wang et al. [21] presented Iterative Non Local Means (INLM) filtering technique for exploiting non-local similarity features from the images to remove salt and pepper noise. In INLM technique, non-local information was exploited from the images to preserve the image details. After identifying the same image patches, the denoising result was estimated iteratively. The simulation outcome showed that the developed INLM technique achieved better denoising performance than the existing techniques in light of SSIM and PSNR value. However, the developed INLM filtering technique is applied only to remove salt and pepper noise, which need to be concentrated on other noises like Gaussian, impulse, etc.

Frosio and Kautz [22] combined Statistical Nearest Neighbors (SNN) with NLM technique for color image denoising. The developed model generates images with superior quality at a lower computational complexity. In the experimental section, the developed NLM-SNN model outperforms the conventional NLM-NN model by means of SSIM, and PSNR on KODAK database. Usually, high SNN value is required to generate the images with superior quality that leads to system complexity. Rakhshanfar and Amer [23] combined different denoisers to achieve high quality images with lower complexity. Initially, three different cascading forms were analyzed that delivers speed quality options. A fast image denoiser; Cascaded Multi-Domain Filter (CMDF) was developed by cascading frequency and pixel domain filters that utilizes the benefits of smaller and larger kernel filters. Lastly, CMDF was cascaded with existing denoisers to attain high quality images with low complexity. In this literature, the developed CMDF model represents the contribution of numerous image pixels in large spatial position that results in blocking artifacts and ringing. Huang, et al. [32], and Huang, et al. [33] developed a Block Matching, and Three Dimensional filter (BM3D) for removing noise from Knowledge enhanced Mobile Video Broadcasting (KMV-Cast). In this literature article, the BM3D filter collects similar image pixels for revealing the patch characteristic, where the collaborative filter preserves the unique feature of every block using hard thresholding. Additionally, an aggregation procedure was carried out for obtaining the estimation results. The simulation results showed that the developed BM3D filter achieved better image denoising performance compared to the existing filtering techniques in terms of PSNR. Tian, et al., [1] introduced an Attention-guided Denoising convolutional neural network (ADNet) for digital image denoising that majorly includes four blocks such as sparse, feature enhancement, attention, and reconstruction block. The common convolutions were used in sparse block for eliminating the Gaussian noise. To improve the expressive abilities of the ADNet model, local and global features were used in feature enhancement block. Next, finely extract the noise information in the attention block to minimize the system complexity. By using the obtained noise map, reconstruction block delivers the denoised image. However, BM3D and ADNet has poor denoising performance, while the digital images are corrupted by high level of noise. To highlight the aforementioned issues, ESNN-SPT model is proposed in this research to improve the performance of image denoising.

3 Methodology

In this research study, the proposed ESNN-SPT model performance is validated on KODAK database. **Link:** http://www.cs.albany.edu/~xypan/research/snr/Kodak.html. KODAK database is collected from Eastman Kodak Company that includes 25 uncompressed Portable Graphics Format (PGF) images with the size of 768×512image pixels [24]. The KODAK dataset is created using Gaussian noise domination with a real noisy image, so it is preferred in this research. The sample images of KODAK database is represented in Fig. 1.

Fig. 1 Sample images of KODAK database

3.1 Enhanced statistical nearest neighbor

Generally, NLM technique averages the same image patches and then aggregates the averages into final denoised image. Let us consider the vector representation of noisy reference patch $\mu_r = [\mu_r^0, \mu_r = [\mu_r^0, \mu_r^1, \ldots \ldots \mu_r^{S^2C-1}]$ and the noisy neighbor patch γ_k. The squared distance of μ_r and γ_k is defined in Eq. (1).

$$d^2(\mu_r, \gamma_k) = \frac{1}{P} \times \sum_{i=0}^{P-1} (\mu_r^i - \gamma_k^i)^2 \tag{1}$$

where, $P = S^2C$ and then define an exponential kernel function $f_k(x)$ [25] for weighting the patch γ_k, as shown in Eq. (2). Usually, the NLM technique effectively cleans the edges, and eliminates the noise with-out losing too many fine structures and details. If the noise level increases, NLM technique deteriorates, and suffers from blurring that leads to loss of image details. This concern is occurred by using same local patches for finding the pixel weights contains noisy pixels. To highlight this concern, an exponential kernel function is introduced in NLM technique to adjust the local structure of image, and to reduce the prediction error in noise free patches for better noise removal.

$$w_{\mu_r,\gamma_k} = e^{-\frac{\max(0, d^2(\mu_r - \gamma_k) - 2\sigma^2}{h^2}} \times f_k(x) \tag{2}$$

where, $f_k(x) = \begin{cases} \exp\left(-\frac{\Omega^2(i,j)}{\sigma^2}\right)\cos\left(\frac{\pi}{2}\frac{\Omega(i,j)}{\sigma}\right)\left(1 - \frac{\Omega^2(i,j)}{\sigma^2}\right)^2, 0 < \Omega(i,j) \le \sigma \\ 0, else \end{cases}$,

h is stated as filtering parameter and it depends on the Gaussian noise σ^2. Then, the estimation of the noise free patch $\hat{\mu}(\mu_r)$ is mathematically defined in Eq. (3). In ESNN technique, the same image patches are determined by calculating the distance between the image patches with similar size of μ_r, as shown in Eq. (4).

$$\hat{\mu}(\mu_r) = \frac{\sum_k w_{\mu_r,\gamma_k} \times \gamma_k}{\sum_k w_{\mu_r,\gamma_k}} \tag{3}$$

$$d^2(\mu_r, \gamma_k) = \left(\frac{2\sigma^2}{P}\right) \times \sum_{i=0}^{P-1} G(0,1)^2 \tag{4}$$

where, γ_k is represented as neighborhood patches, μ is indicated as mean, σ^2 is stated as Gaussian noise variance, $G(\mu, \sigma^2)$ is represented as Gaussian random value and the sum of squared normal value P has x_P^2 distribution, so $d^2(\mu_r, \gamma_k) \sim \left(\frac{2\sigma^2}{P}\right) \times x_P^2$, as represented in Eq. (5).

$$E\left[d^2(\mu_r, \gamma_k)\right] = 2\sigma^2 \tag{5}$$

The ESNN technique supports intuition with analytical evidence in order to deal with the tractable issues. In this study, a reference patch 1×1 with noise free image pixel μ is contaminated with Gaussian noise σ^2 with variance, $\mu_r \sim G(\mu, \sigma^2)$. Next, the probability density function P and the cumulative density function $\emptyset$ are applied on the noisy reference patch μ_r. The probability and the cumulative density functions are mathematically indicated in the Eqs. (6) and (7).

$$P(\mu_r < x) = \Phi_{\mu,\sigma^2}(x) = \frac{1}{2} \times \left[1 + erf\left(\frac{x - \mu}{\sqrt{2\sigma}}\right)\right] \tag{6}$$

$$\emptyset_{\mu,\sigma^2}(x) = \Phi'_{\mu,\sigma^2}(x) = \frac{1}{\sqrt{2\pi\sigma}} e^{-0.5\left[\frac{(x-\mu)}{\sigma}\right]^2} \tag{7}$$

Let us consider, noisy neighbors $N \rightarrow \{\gamma_k\}, k = 1, ..N$, where N replicates μ and it is distribution is denoted as $G(\mu, \sigma^2)$. The probability density function P and the cumulative density function $\emptyset$ of $\{\gamma_k\}, k = 1, \ldots .N$ is indicated in the Eqs. (8) and (9).

$$P\left(\gamma_k < x\right) = \Phi_{mix}(x) = p_r\Phi_{\mu,\sigma^2}(x) + p_f\Phi_{\mu_f,\sigma^2}(x) \tag{8}$$

$$\emptyset_{mix}(x) = \Phi_{mix}(x)' = p_r\emptyset_{\mu,\sigma^2}(x) + p_f\emptyset_{\mu_f,\sigma^2}(x) \tag{9}$$

Additionally, the simplified estimator $\hat{\mu}\left(\mu_r\right)$ is mathematically represented in Eq. (10).

$$\hat{\mu}\left(\mu_r\right) = \frac{1}{N_n}\sum_{k=1,\ldots N_n}\gamma_k \tag{10}$$

where, γ_k is represented as noisy neighbor patches, and p_f is represented as false matches, where its distribution is $G\left(\mu_f,\sigma^2\right)$. For a reference patch μ_r, the prediction error of $\hat{\mu}\left(\mu_r\right)$ is decomposed into bias and variance terms that are derived using the Eqs. (11–13)

$$\in^2\left(\mu_r\right) = \int_{\hat{\mu}}(\hat{\mu}-\mu)^2p(\hat{\mu})d\hat{\mu} = \in^2_{bias}\left(\mu_r\right) + \in^2_{var}\left(\mu_r\right) \tag{11}$$

$$\in^2_{bias}\left(\mu_r\right) = \int_{\hat{\mu}}(E[\hat{\mu}]-\mu)^2p(\hat{\mu})d\hat{\mu} = \{E\left[\hat{\mu}\left(\mu_r\right)-\mu\right]\}^2 \tag{12}$$

$$\in^2_{var}\left(\mu_r\right) = \int_{\hat{\mu}}(\hat{\mu}-E[\hat{\mu}])^2p(\hat{\mu})d\hat{\mu} = Var\left[\hat{\mu}\left(\mu_r\right)\right] \tag{13}$$

where, $p(\hat{\mu})$ is indicated as the probability density function of $\hat{\mu}$. Next, eliminate the dependency of $\hat{\mu}\left(\mu_r\right)$ from μ_r for notation clarity with-in the integrals and $p(\hat{\mu})$. Then, estimate the total error of the estimator by utilizing the distribution of μ_r, as mentioned in the Eqs. (14–16).

$$\in^2 = \in^2_{bias} + \in^2_{var} \tag{14}$$

$$\in^2_{bias} = \int_{\mu_r}\in^2_{bias}\left(\mu_r\right)\emptyset_{\mu,\sigma^2}\left(\mu_r\right)d\mu_r \tag{15}$$

$$\in^2_{var} = \int_{\mu_r}\in^2_{var}\left(\mu_r\right)\emptyset_{\mu,\sigma^2}\left(\mu_r\right)d\mu_r \tag{16}$$

When the neighbors are collected using NN and SNN techniques, the set $\left\{\gamma_k\right\}, k = 1\ldots N_n$ contains N_n samples. The statistical distribution of $E\left[\hat{\mu}\left(\mu_r\right)\right]$ and $Var\left[\hat{\mu}\left(\mu_r\right)\right]$ are estimated using the Eqs. (12) and (13) to determine the estimation error. Let us consider $\delta = \left|\gamma N_n\left(\mu_r\right) - \mu_r\right|$ that represents the distance of N_n^{th} nearest neighbors from μ_r. Each γ_k is independent of other factors apart from a normalization factor ξ. In $[\mu_r-\delta, \mu_r+\delta]$ interval, the probability of N_n neighbors is the product of 3 terms;

- Probability of $N_n - 1$ samples lies in $[\mu_r-\delta, \mu_r+\delta]$.
- Probability of $N_n{}^{th}$ neighbor lies at distance δ and μ_r.
- Probability of $N - N_n$ samples lies outside of the interval $[\mu_r-\delta, \mu_r+\delta]$.

The probability of finding N_n samples with the distance δ from μ_r is mathematically shown in Eq. (17).

$$p(\delta) = \xi \times pin(\delta)^{N_n-1}p_{bou}(\delta)\left[1-pin(\delta)\right]^{N-N_n} \tag{17}$$

where,

$$pin(\delta) = \Phi_{mix}\left(\mu_r+\delta\right) - \Phi_{mix}\left(\mu_r-\delta\right)$$

$$p_{bou}(\delta) = \emptyset_{mix}\left(\mu_r-\delta\right) - \emptyset_{mix}\left(\mu_r+\delta\right)$$

The normalization factor ξ is determined by forcing $\int_0^{+\infty}p(\delta)d\delta = 1$. By utilizing Eq. (17), $E\left[\hat{\mu}\left(\mu_r\right)\right]$ and the expected value of the interval are estimated as given in Eq. (18).

$$E\left[\hat{\mu}\left(\mu_r\right)\right] = \frac{\Delta\delta}{N_n}\sum_{\delta}\sum_{k=1..N_n}E\left[\frac{\gamma_k}{\delta}\right]\times p(\delta) \tag{18}$$

After marginalizing over δ, each N_n neighbors of γ_k lies in the interval $[\mu_r-\delta, \mu_r+\delta]$. Though, $N_n - 1$ neighbor is a combination of truncated Gaussian $G'\left(\mu,\sigma^2,\mu_r-\delta,\mu_r+\delta\right)$ with probability p_r and 2^{nd} truncated Gaussian $G'\left(\mu_f,\sigma^2,\mu_r-\delta,\mu_r+\delta\right)$ with probability p_f. The expected value of $\hat{\mu}\left(\mu_r\right)$ is determined by utilizing Eq. (18) and the variance of $\hat{\mu}\left(\mu_r\right)$ is computed by marginalizing the value δ that is mathematically defined in Eq. (19).

$$\begin{aligned} Var\left[\hat{\mu}\left(\mu_r\right)\right] &= \int_{-\infty}^{+\infty}(\hat{\mu}-E[\hat{\mu}])^2p(\hat{\mu})d\hat{\mu} \\ &= \int_{-\infty}^{+\infty}(\hat{\mu}-E[\hat{\mu}])^2\int_0^{+\infty}\{p\left(\frac{\hat{\mu}}{\delta}\right)p(\delta)d\delta\}d\hat{\mu} \\ &= \int_0^{+\infty}\{\int_{-\infty}^{\infty}(\hat{\mu}-E[\hat{\mu}])^2p\left(\frac{\hat{\mu}}{\delta}\right)d\hat{\mu}\}p(\delta)d\delta \end{aligned} \tag{19}$$

Once again restore the numerical integration by adding and subtracting $E[\hat{\mu}|\delta]$, as denoted in Eq. (20).

$$Var\left[\hat{\mu}\left(\mu_r\right)\right] \cong \Delta\delta\sum_{\delta}\sum_{k=1..N_n}\{\frac{\text{var}\left[\gamma_k|\delta\right]}{N_n^2} + (E\left[\gamma_k|\delta\right] - E[\hat{\mu}])^2\}.p(\delta) \tag{20}$$

Then, collect the neighbor's square distance from the reference patch as an alternative to NN and SNN techniques. The ESNN patch $\left\{\gamma_k\right\}, k = 1, ..N_n$ is minimized by using the Eq. (21).

$$\left|d^2\left(\mu_r,\gamma_k\right) - o.2\sigma^2\right|, o = 1 \tag{21}$$

where, o is stated as additional off-set parameter. Next, $E\left[\hat{\mu}\left(\mu_r\right)\right]$ and, $Var\left[\hat{\mu}\left(\mu_r\right)\right]$ are estimated to compare the prediction error of NN, SNN and ESNN techniques. Lastly, Fischer's approximation $\left(\sqrt{2x_P^2} \cong G\left(\sqrt{2P-1},1\right)\right.$ is applied in Eq. (4) for a single patch $P = 1$, where it is indicated in Eq. (22).

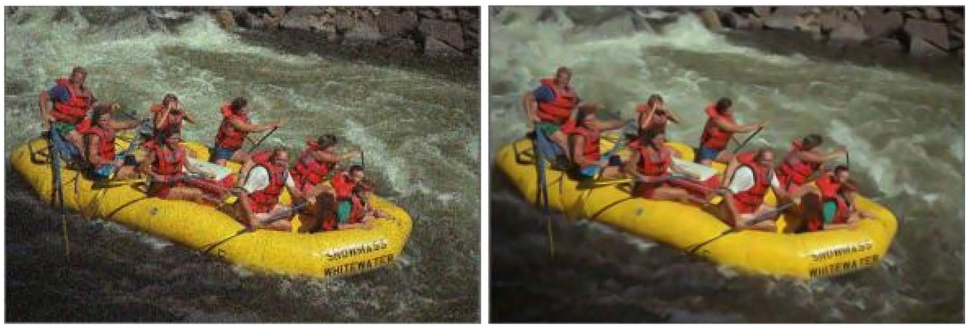

(a) (b)

Fig. 2 **a** Noisy image, and **b** Output of ESNN

$$d^2(\mu_r, \gamma) \cong \sigma \times \sqrt{2P-1} + G(0, \sigma^2) = \sigma + G(0, \sigma^2) \quad (22)$$

The ESNN technique effectively diminishes the prediction error in noise free patches that deblurs the lower contrast image details with minimum signal to noise ratio. The output of ESNN technique is graphically indicated in Fig. 2. The ESNN technique has an issue of shift-invariant, so the SPT is introduced in this research. The SPT is a multi-orientation and multi-scale transformation technique, which delivers useful frond end for image denoising application. The explanation about SPT is given in Sect. 3.2.

3.2 Steerable pyramid transform

In this section, SPT is applied on the output image of ESNN technique that divides the image into several orientations and scales. SPT is a recursive and multi-scale wavelet transform that has derivative operations in several directions, which involves in variable sizes [26]. Initially, the SPT decomposes the output image of ESNN into sub-bands of different orientations and scales, where the orientation band-width is equal to $2\pi/o$, o is represented as number of orientations. Hence, the resultant sub-bands are rotation invariant and translation. Further, low pass filter L_0 and high pass filter H_0 are applied to decompose the images into lower and higher frequency components. Again, the lower frequency components are decomposed into 2 oriented band-pass components and lower frequency components by employing band pass filters B_0andB_1, and low pass filter L_1. Next, the lower frequency part is down sampled by the factor of 2. The shaded part in the resultant image is inserted into the un-filled small circle to generate recursive steerable pyramid. Output of frequency domain is mathematically defined in Eq. (23).

$$\hat{I}(\vec{w}) = \left\{ \left|H_0(\vec{w})\right|^2 + \left|L_0(\vec{w})\right|^2 \left(\left|L_1(\vec{w})\right|^2 + \sum_{K=0}^{N} \left|B_K(\vec{w})\right|^2 \right) \right\} I(\vec{w}) + AT \quad (23)$$

where, AT is stated as aliasing terms. L_1 should have zero magnitude response for the frequencies that are higher than the 1-4th of the sampling frequencies to avoid aliasing terms. In SPT, the orientation of the filters need to satisfy the following conditions,

- Filter is rotated and copied to generate another filters, where all the filters are copy-rotated of their counterparts.
- A filter with any orientation is generated based on the linear combination of the filters.

By increasing the number of orientations (derivative degree), number of pyramid levels are increased that delivers finer orientation and scaler tuning of image. After transforming the images, hard thresholding T_H is applied to deliver the image with better visibility level. Hard thresholding is mathematically defined in Eq. (24). The output of SPT is graphically denoted in Fig. 3.

$$T_H = \begin{cases} x \, for \, |x| \geq t \\ 0 \, in \, all \, other \, regions \end{cases}, \; t \, is \, a \, threshold \, value \quad (24)$$

3.3 Computational complexity of the research

At every pixel, weight to all other image pixel is computed, and then the noise free image pixels are effectively determined by SPT technique that yields the computational complexity of linear $O(P_d \mu_n)$, where, P_d indicates patch size and μ_n states number of noise free pixels in an image. By eliminating the noisy pixels by SPT technique

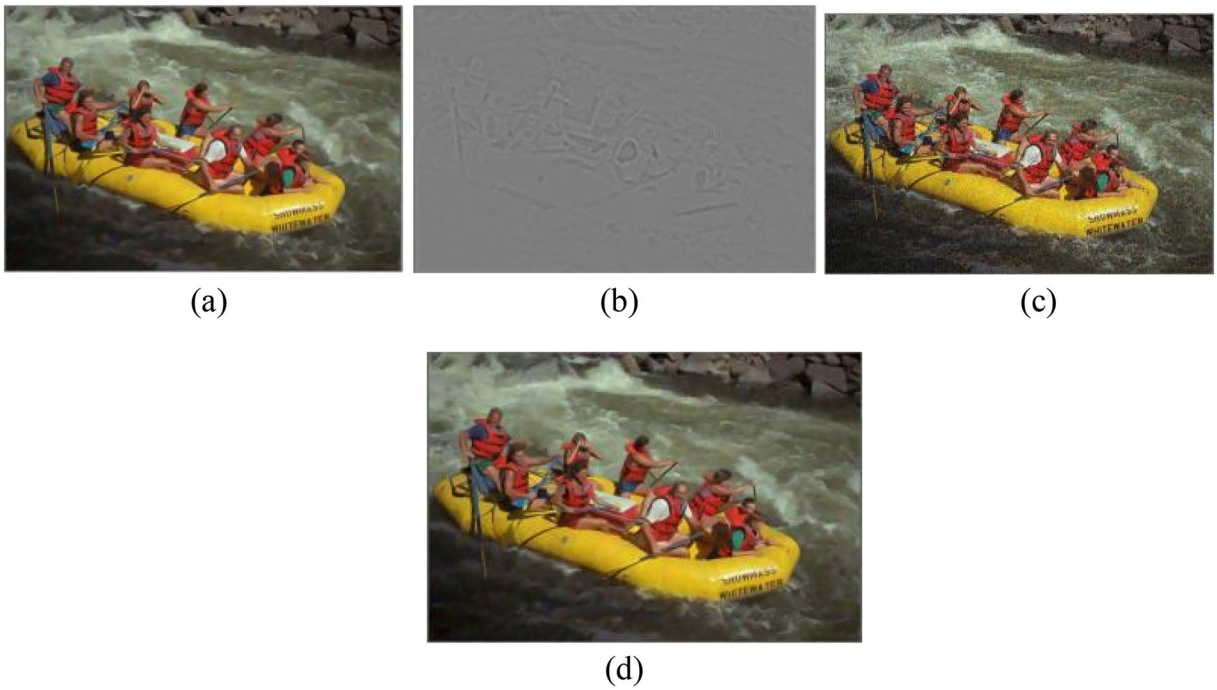

Fig. 3 **a** Output of ESNN, **b** decomposed image, **c** Output of SPT, and **d** Output of SPT with hard thresholding

with hard thresholding, the computational cost is also linear in this research.

4 Experimental results

The proposed ESNN-SPT model is simulated using MATLAB (2018a) environment with the system requirements; **Operating System:** windows 10, **RAM:** 8 GB, and **processor:** Intel core i7. In this work, the proposed ESNN-SPT model performance is compared with the existing models; ADNet [1], ADNet-B [1] and NLM-SNN [22] by varying the sigma of Gaussian noise. Additionally, the performance of the proposed ESNN-SPT model was analyzed in terms of MSSIM, PSNR, FSIM, SSIM, and $FSIM_c$. PSNR value is calculated using Mean Square Error (MSE), where the high PSNR value represents the better quality of denoised image $k'(x, y)$. The general formula of PSNR is represented in Eq. (25).

$$PSNR = 20log_{10}\left(\frac{max(k(x,y))}{\sqrt{MSE}}\right) \tag{25}$$

where, $MSE = \frac{1}{mn}\sum_{x=0}^{m-1}\sum_{y=0}^{n-1} k(x,y) - k'(x,y)^2$, $k(x, y)$ is denoted as noisy image, inclusion of Gaussian noise with different sigma ranges, $k'(x, y)$ is represented as denoised image and the dimension of the image is denoted as m and n. Additionally, SSIM and MSSIM are the common performance measures that are used to estimate the similarity between noisy and denoised images [27–29]. The SSIM and MSSIM are mathematically defined in the Eqs. (26) and (27).

$$SSIM(x,y) = \frac{\left(2\mu_x\mu_y + c_1\right)\left(2\sigma_{xy} + c_2\right)}{\left(\mu_{x^2} + \mu_{y^2} + c_1\right)\left(\sigma_{x^2} + \sigma_{y^2} + c_2\right)} \tag{26}$$

$$MSSIM = \frac{1}{window}\sum_{x,y=1}^{window}(SSIM(x,y)) \tag{27}$$

where, σ is indicated as standard deviation, μ is represented as mean value, *window* is denoted as number of windows in the noisy and denoised image, c_1 and c_2 are stated as constants. In image denoising, FSIM is one of the fine image quality measure [30], where the computation of FSIM index includes two phases. In the first phase, local similarity map of the image is computed and then the similarity maps are pooled into a single similarity score in the second phase. $FSIM_c$ is the extension of FSIM index that incorporates the chromatic information of the image in a straight-forward manner.

4.1 Quantitative analysis

In this research, the original digital image is contaminated with Gaussian noise and then a model is proposed to reconstruct the noisy image with better visibility level. Gaussian

Table 1 Performance analysis of ESNN-SPT model with the noise range $\sigma = 15$

σ=15												
Measures	Methods	Kod01	Kod02	Kod03	Kod04	Kod05	Kod07	Kod11	Kod13	Kod15	Kod18	Kod23
PSNR	SNN	26.61	31.50	32.39	30.64	27.14	31.35	29.55	25.47	31.15	27.69	33.42
	SPT	24.60	24.62	24.63	24.63	24.59	24.63	24.62	24.59	24.62	24.60	24.64
	ESNN	26.61	31.68	32.63	30.80	27.14	31.55	29.60	25.45	31.31	27.73	33.80
	ESNN-SPT	**27.37**	**31.81**	**33.05**	**31.10**	**28.27**	**31.73**	**30**	**26.26**	**31.62**	**27.98**	**33.93**
SSIM	SNN	0.87	0.98	0.95	0.96	0.94	0.95	0.90	0.85	0.94	0.87	0.96
	SPT	0.80	0.94	0.66	0.80	0.95	0.69	0.64	0.81	0.68	0.67	0.74
	ESNN	0.87	0.98	0.96	0.96	0.96	0.96	0.90	0.86	0.94	0.88	0.97
	ESNN-SPT	**0.88**	**0.98**	**0.96**	**0.97**	**0.97**	**0.96**	**0.90**	**0.87**	**0.94**	**0.88**	**0.97**
MSSIM	SNN	0.91	0.85	0.92	0.90	0.95	0.96	0.90	0.88	0.91	0.90	0.95
	SPT	0.87	0.57	0.62	0.69	0.90	0.77	0.73	0.86	0.64	0.77	0.67
	ESNN	0.91	0.86	0.94	0.90	0.95	0.96	0.90	0.88	0.92	0.90	0.96
	ESNN-SPT	**0.92**	**0.86**	**0.94**	**0.91**	**0.95**	**0.96**	**0.91**	**0.89**	**0.93**	**0.91**	**0.96**
FSIM	SNN	0.99	0.99	0.99	0.99	0.99	0.99	0.99	0.99	0.99	0.99	0.99
	SPT	0.99	0.99	0.99	0.99	0.99	0.99	0.99	0.99	0.99	0.99	0.98
	ESNN	0.99	0.99	0.99	0.99	0.99	0.99	0.99	0.99	0.99	0.99	0.99
	ESNN-SPT	**0.99**	**0.99**	**0.99**	**0.99**	**0.99**	**0.99**	**0.99**	**0.99**	**0.99**	**0.99**	**0.99**
$FSIM_c$	SNN	0.99	0.99	0.99	0.99	0.99	0.99	0.99	0.99	0.99	0.99	0.99
	SPT	0.99	0.99	0.99	0.99	0.99	0.99	0.99	0.99	0.99	0.99	0.98
	ESNN	0.99	0.99	0.99	0.99	0.99	0.99	0.99	0.99	0.99	0.99	0.99
	ESNN-SPT	**0.99**	**0.99**	**0.99**	**0.99**	**0.99**	**0.99**	**0.99**	**1**	**0.99**	**0.99**	**0.99**

Bold values indicate the results of proposed method compared to other existing methods

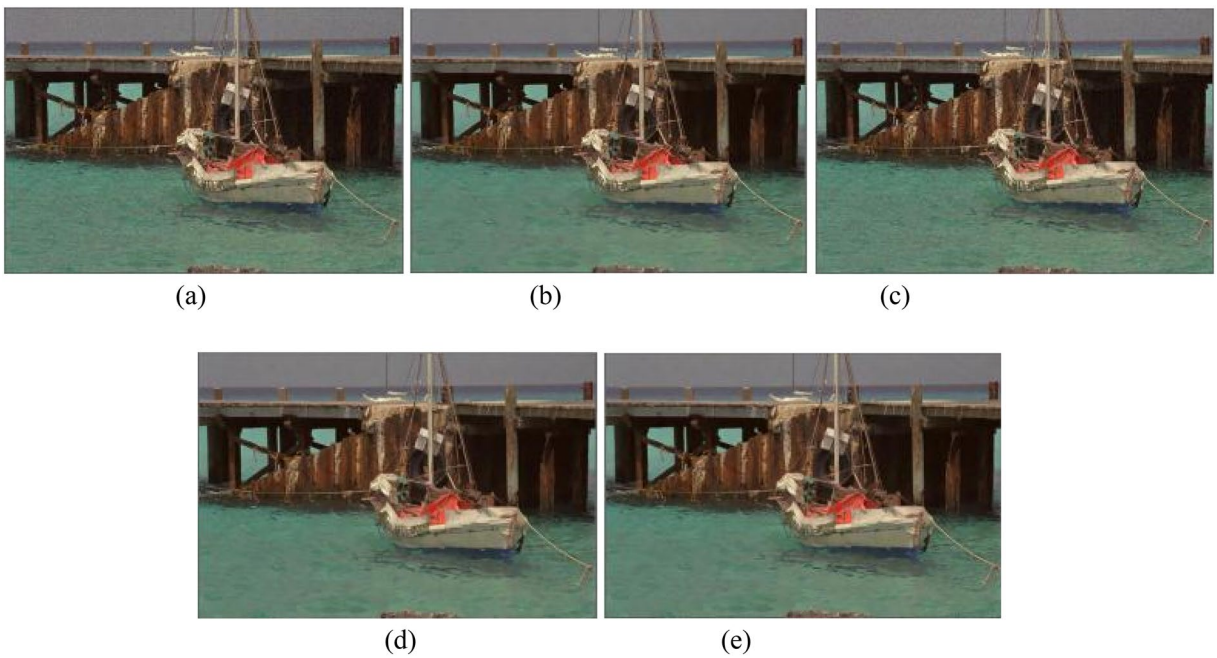

Fig. 4 $\sigma = 15$, **a** Noisy image, **b** Output image of SNN, **c** Output image of SPT, **d** Output image of ESNN, and **e** Output image of ESNN-SPT

noise is a statistical or widespread noise that have probability density function equal to Gaussian distribution [31]. By inspecting Table 1, the proposed ESNN-SPT model achieved better denoising performance compared to the existing models such as Statistical Nearest Neighbor (SNN), Steerable Pyramid Transform (SPT) and Enhanced Statistical Nearest

Neighbor (ESNN) by means of MSSIM, PSNR, FSIM, SSIM and $FSIM_c$. In this research work, KODAK database (25 uncompressed color images) is utilized to validate the performance of proposed and comparative models. In the case of $\sigma = 15$, the proposed ESNN-SPT model achieved maximum PSNR value of 33.93 dB, SSIM value of 0.98, MSSIM value of 0.96, FSIM value of 0.99 and $FSIM_c$ value of 1. The SPT is a linear multi-orientation and multi scale image decomposition technique that delivers a useful front end for image denoising applications. Figure 4 represents the output image of proposed and existing models, where Fig. 4a is a noisy image, which is contaminated with the Gaussian noise of $\sigma = 15$. Respectively, the Figs. 4b, c, d, and e represents the output image of SNN, SPT, ESNN and ESNN-SPT models.

In Table 2, the proposed ESNN-SPT model performance is analyzed with the noise range of $\sigma = 25$. By inspecting Table 2, the proposed ESNN-SPT model achieved maximum PSNR value of 32.39 dB, SSIM value of 0.98, MSSIM value of 0.95, FSIM value of 0.99 and $FSIM_c$ value of 0.99. Compared to the comparative models (SNN, SPT and ESNN), the proposed ESNN-SPT model delivered the denoised image with better visibility level. The proposed ESNN-SPT model preserve the fine details and edges more effectively. The advantage of ESNN-SPT model is evident in the case of color image, while noise to noise matching is occurred. The visual analysis shows that the ESNN-SPT model achieved comparable image denoising performance related to the comparative models with a low computational complexity. Output image of proposed and existing models are denoted in Fig. 5. In that, Fig. 5a represents the noisy image, which is contaminated with the Gaussian noise of $\sigma = 25$. Correspondingly, the Fig. 5b, c, d, and e indicates the output image of SNN, SPT, ESNN and ESNN-SPT models.

In addition, Table 3 analysis the performance of proposed ESNN-SPT model and the existing models (SNN, SPT, and ESNN) by means of MSSIM, PSNR, FSIM, SSIM and $FSIM_c$ with the Gaussian noise range of $\sigma = 35$. By investigating Table 3, the proposed ESNN-SPT model achieved better denoising performance with maximum PSNR value of 31.07, SSIM value of 0.97, MSSIM value of 0.92, FSIM value of 0.99 and $FSIM_c$ value of 0.99. The effectiveness of the proposed and comparative models are analyzed on KODAK database that includes 25 uncompressed PNG color images of size 768×512 pixels. Figure 6 states the output images, which are contaminated with the Gaussian noise of $\sigma = 35$.

4.2 Comparative analysis

The comparative analysis of the proposed and the existing models are indicated in the Tables 4, 5, and 6. Frosio

Table 2 Performance analysis of ESNN-SPT model with the noise range $\sigma = 25$

σ=25												
Measures	Methods	Kod01	Kod02	Kod03	Kod04	Kod05	Kod07	Kod11	Kod13	Kod15	Kod18	Kod23
PSNR	SNN	24.57	29.89	30.80	30.59	24.95	29.37	29.51	23	29.44	27.70	30.97
	SPT	20.18	20.17	20.19	24.63	20.18	20.20	24.61	20.17	20.18	24.61	20.20
	ESNN	24.63	30.35	31.37	30.76	25.01	29.82	29.57	23.04	29.80	27.75	31.68
	ESNN-SPT	**26.15**	**30.73**	**32.27**	**31.10**	**26.06**	**31.10**	**30.98**	**24.98**	**30.63**	**28**	**32.39**
SSIM	SNN	0.82	0.98	0.92	0.96	0.84	0.92	0.90	0.80	0.90	0.98	0.94
	SPT	0.62	0.86	0.48	0.80	0.60	0.50	0.64	0.64	0.49	0.86	0.57
	ESNN	0.82	0.98	0.94	0.96	0.85	0.94	0.90	0.80	0.92	0.98	0.95
	ESNN-SPT	**0.84**	**0.98**	**0.94**	**0.97**	**0.86**	**0.95**	**0.90**	**0.81**	**0.92**	**0.98**	**0.96**
MSSIM	SNN	0.86	0.78	0.87	0.90	0.92	0.93	0.90	0.82	0.86	0.90	0.91
	SPT	0.73	0.37	0.45	0.69	0.79	0.62	0.73	0.72	0.48	0.77	0.50
	ESNN	0.86	0.80	0.90	0.90	0.92	0.94	0.90	0.82	0.89	0.90	0.93
	ESNN-SPT	**0.89**	**0.80**	**0.91**	**0.91**	**0.93**	**0.95**	**0.90**	**0.83**	**0.89**	**0.91**	**0.93**
FSIM	SNN	0.99	0.98	0.99	0.99	0.99	0.99	0.99	0.99	0.99	0.99	0.99
	SPT	0.99	0.97	0.97	0.99	0.99	0.99	0.99	0.99	0.98	0.99	0.97
	ESNN	0.99	0.98	0.99	0.99	0.99	0.99	0.99	0.99	0.99	0.99	0.99
	ESNN-SPT	**0.99**	**0.98**	**0.99**	**0.99**	**0.99**	**0.99**	**0.99**	**0.99**	**0.99**	**0.99**	**0.99**
$FSIM_c$	SNN	0.99	0.98	0.99	0.99	0.99	0.99	0.99	0.99	0.99	0.99	0.99
	SPT	0.99	0.97	0.97	0.99	0.99	0.99	0.99	0.99	0.98	0.99	0.97
	ESNN	0.99	0.98	0.99	0.99	0.99	0.99	0.99	0.99	0.99	0.99	0.99
	ESNN-SPT	**0.99**	**0.98**	**0.99**	**0.99**	**0.99**	**0.99**	**0.99**	**0.99**	**0.99**	**0.99**	**0.99**

Bold values indicate the results of proposed method compared to other existing methods

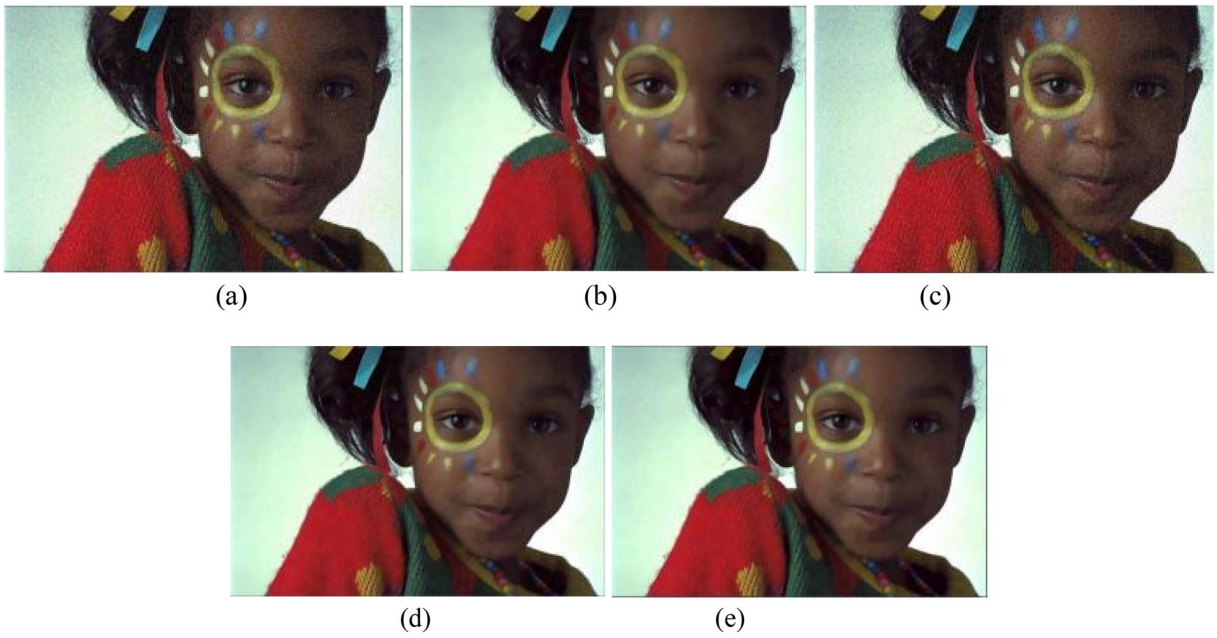

Fig. 5 σ =25, **a** Noisy image, **b** Output image of SNN, **c** Output image of SPT, **d** Output image of ESNN, and **e** Output image of ESNN-SPT

Table 3 Performance analysis of ESNN-SPT model with the noise range σ =35

σ=35												
Measures	Methods	Kod01	Kod02	Kod03	Kod04	Kod05	Kod07	Kod11	Kod13	Kod15	Kod18	Kod23
PSNR	SNN	24.10	28.55	29.49	28.15	23.99	28.15	26.20	21.76	28.25	24.53	29.17
	SPT	17.27	17.25	17.28	17.27	17.25	17.28	17.27	17.25	17.26	17.25	17.28
	ESNN	24.25	29.26	30.38	28.88	24.11	28.83	26.47	21.84	28.82	24.75	30.16
	ESNN-SPT	**24.76**	**29.42**	**30.59**	**29.41**	**24.92**	**29.32**	**26.96**	**22.38**	**29.35**	**25.54**	**31.07**
SSIM	SNN	0.78	0.97	0.88	0.92	0.80	0.88	0.79	0.76	0.86	0.76	0.91
	SPT	0.48	0.76	0.36	0.48	0.46	0.36	0.32	0.50	0.36	0.38	0.45
	ESNN	0.79	0.97	0.92	0.94	0.81	0.92	0.82	0.77	0.89	0.79	0.94
	ESNN-SPT	**0.80**	**0.97**	**0.92**	**0.95**	**0.81**	**0.92**	**0.82**	**0.78**	**0.89**	**0.80**	**0.94**
MSSIM	SNN	0.83	0.70	0.82	0.81	0.89	0.89	0.79	0.77	0.81	0.80	0.86
	SPT	0.59	0.25	0.34	0.37	0.68	0.49	0.44	0.59	0.38	0.45	0.39
	ESNN	0.83	0.74	0.86	0.84	0.90	0.92	0.81	0.78	0.85	0.82	0.90
	ESNN-SPT	**0.84**	**0.74**	**0.86**	**0.84**	**0.90**	**0.92**	**0.81**	**0.80**	**0.86**	**0.87**	**0.90**
FSIM	SNN	0.99	0.98	0.99	0.81	0.99	0.99	0.98	0.99	0.99	0.98	0.99
	SPT	0.99	0.96	0.96	0.37	0.99	0.98	0.98	0.99	0.97	0.99	0.95
	ESNN	0.99	0.98	0.99	0.84	0.99	0.99	0.98	0.99	0.99	0.98	0.99
	ESNN-SPT	**0.99**	**0.98**	**0.99**	**0.84**	**0.99**	**0.99**	**0.98**	**0.99**	**0.99**	**0.99**	**0.99**
$FSIM_c$	SNN	0.99	0.98	0.99	0.99	0.99	0.99	0.98	0.99	0.99	0.98	0.99
	SPT	0.99	0.96	0.96	0.97	0.99	0.98	0.98	0.99	0.97	0.99	0.95
	ESNN	0.99	0.98	0.99	0.98	0.99	0.99	0.98	0.99	0.99	0.98	0.99
	ESNN-SPT	**0.99**	**0.98**	**0.99**	**0.98**	**0.99**	**0.99**	**0.98**	**0.99**	**0.99**	**0.99**	**0.99**

Bold values indicate the results of proposed method compared to other existing methods

and Kautz, [22] combined SNN with NLM technique for color image denoising. The developed SNN technique collects the nearest neighbors in the images to estimate the noise free patches in NLM that improves the visible level of the images. In addition to this, Tian, et al., [1] introduced ADNet, and ADNet-B models for digital

Fig. 6 σ =35, **a** Noisy image, **b** Output image of SNN, **c** Output image of SPT, **d** Output image of ESNN, and **e** Output image of ESNN-SPT

Table 4 Comparative analysis of the proposed and existing model with the noise range σ = 5and10

Denoising models	σ=5					σ=10				
	PSNR	SSIM	MSSIM	FSIM	$FSIM_c$	PSNR	SSIM	MSSIM	FSIM	$FSIM_c$
$NLM-SNN^{361}_{.0}$[22]	38.34	0.9851	0.9921	0.9941	0.9939	34.84	0.9634	0.9804	0.9814	0.9811
$NLM-SNN^{16}_{.0}$[22]	38.08	0.9847	0.9919	0.9949	0.9947	33.96	0.958	0.9773	0.9861	0.9856
$NLM-SNN^{16}_{.1}$[22]	38.08	0.9847	0.9919	0.9949	0.9947	33.96	0.958	0.9773	0.9861	0.9856
$NLM-SNN^{16}_{.35}$[22]	38.08	0.9847	0.9919	0.9949	0.9947	33.96	0.958	0.9773	0.9861	0.9856
$NLM-SNN^{16}_{.65}$[22]	38.14	0.985	0.992	0.9949	0.9947	34.19	0.961	0.9789	0.9861	0.9857
$NLM-SNN^{16}_{.8}$[22]	38.23	0.9854	0.9922	0.9948	0.9946	34.51	0.9639	0.9805	0.9856	0.9852
$NLM-SNN^{16}_{.9}$[22]	38.28	0.9854	0.9923	0.9946	0.9945	34.66	0.9645	0.9809	0.9845	0.9841
$NLM-SNN^{16}_{1.0}$[22]	38.29	0.9852	0.9921	0.9944	0.9942	34.71	0.9635	0.9803	0.9828	0.9824
ESNN-SPT	**40.15**	**0.9889**	**0.9943**	**0.9982**	**0.9981**	**35.93**	**0.9747**	**0.9886**	**0.9985**	**0.9985**

Bold values indicate the results of proposed method compared to other existing methods

Table 5 Comparative analysis of the proposed and existing model with the noise range σ = 20and40

Denoising models	σ=20					σ=40				
	PSNR	SSIM	MSSIM	FSIM	$FSIM_c$	PSNR	SSIM	MSSIM	FSIM	$FSIM_c$
$NLM-SNN^{361}_{.0}$[22]	31.18	0.9109	0.9505	0.9475	0.9468	27.71	0.8184	0.8893	0.8856	0.8844
$NLM-SNN^{16}_{.0}$[22]	29.21	0.8802	0.9343	0.9646	0.9633	25.38	0.7522	0.8591	0.9237	0.9206
$NLM-SNN^{16}_{.1}$[22]	29.21	0.8802	0.9343	0.9646	0.9633	25.38	0.7522	0.8591	0.9237	0.9206
$NLM-SNN^{16}_{.35}$[22]	29.21	0.8802	0.9343	0.9646	0.9633	25.38	0.7522	0.8591	0.9237	0.9206
$NLM-SNN^{16}_{.65}$[22]	29.75	0.8948	0.942	0.9653	0.9641	25.38	0.7522	0.8591	0.9237	0.9206
$NLM-SNN^{16}_{.8}$[22]	30.45	0.9086	0.9493	0.9631	0.9621	25.38	0.7522	0.8591	0.9237	0.9206
$NLM-SNN^{16}_{.9}$[22]	30.81	0.9119	0.9511	0.9585	0.9576	25.49	0.758	0.8624	0.9243	0.9213
$NLM-SNN^{16}_{1.0}$[22]	30.93	0.9084	0.949	0.951	0.9503	26.38	0.7942	0.8813	0.9248	0.9223
ESNN-SPT	**31.88**	**0.9686**	**0.9513**	**0.9942**	**0.9942**	**29.87**	**0.9630**	**0.9058**	**0.9885**	**0.9865**

Bold values indicate the results of proposed method compared to other existing methods

image denoising, where the developed models includes four blocks; sparse, feature enhancement, attention, and reconstruction block to obtain denoise image. Compared to these existing models, ESNN-SPT showed better

Table 6 Comparative analysis of the proposed and existing model with the noise range $\sigma = 15, 35$and50

Mean PSNR value			
Denoising models	$\sigma = 15$	$\sigma = 35$	$\sigma = 50$
ADNet [1]	34.76	30.68	29.10
ADNet-B [1]	34.53	30.44	28.81
ESNN-SPT	**35.18**	**30.91**	**29.72**

Bold values indicate the results of proposed method compared to other existing methods

performance in the homogeneous areas of the images. In this research, KODAK database is undertaken to evaluate the performance of the existing and the proposed model with the noise ranges (0, 0.1, 0.35, 0.65, 0.8. 0.9, and 1), $\sigma = (5, 10, 15, 20, 35, 40and50)$ and the neural network neighbors are fixed as 361 and 16. In this research study, the performance of the existing and proposed model is validated by means of PSNR, MSSIM, SSIM, FSIM, and $FSIM_{c.}$ By inspecting the Tables 4, 5 and 6, the proposed ESNN-SPT model outperforms the existing models; SNN-NLM, ADNet, and ADNet-B by means of PSNR, MSSIM, SSIM, FSIM and $FSIM_c$ with different $\sigma = 5$, 10, 15, 20, 35, 40, and 50 of Gaussian noise.

5 Conclusion

In this research paper, an ESNN-SPT model is proposed along with hard thresholding technique to further diminish Gaussian noise in the color images. The proposed ESNN-SPT model effectively preserves the information bearing structures like textures and edges to achieve better visual quality images. In this research, the proposed ESNN-SPT model performance is analyzed on KODAK database, where the acquired color images are contaminated with different Gaussian noise level. In the experimental step, the proposed ESNN-SPT model achieved effective denoising performance by means of MSSIM, PSNR, FSIM, SSIM, and $FSIM_c$. Compared to NLM-SNN, ADNet, and ADNet-B models, the proposed ESNN-SPT model showed a maximum of 2.07 dB and a minimum of 0.7 dB improvement in PSNR. In future work, a new deep learning technique can be included in the proposed ESNN-SPT model to further improve the performance of image denoising.

Funding This study was not funded by any organization.

Declarations

Conflict of interest The authors declare that they have no conflict of interest.

References

1. Tian C, Xu Y, Li Z, Zuo W, Fei L, Liu H (2020) Attention-guided CNN for image denoising. Neural Netw 124:117–129. https://doi.org/10.1016/j.neunet.2019.12.024
2. Tian C, Xu Y, Zuo W (2020) Image denoising using deep CNN with batch renormalization. Neural Netw 121:461–473. https://doi.org/10.1016/j.neunet.2019.08.022
3. Thanh DNH, Hien NN, Prasath S (2020) Adaptive total variation L1 regularization for salt and pepper image denoising. Optik 208:163677. https://doi.org/10.1016/j.ijleo.2019.163677
4. Valsesia D, Fracastoro G, Magli E (2020) Deep graph-convolutional image denoising. IEEE Trans Image Process 29:8226–8237. https://doi.org/10.1109/TIP.2020.3013166
5. Yang X, Xu Y, Quan Y, Ji H (2020) Image denoising via sequential ensemble learning. IEEE Trans Image Process 29:5038–5049. https://doi.org/10.1109/TIP.2020.2978645
6. Hou Y, Xu J, Liu M, Liu G, Liu L, Zhu F, Shao L (2020) NLH: a blind pixel-level non-local method for real-world image denoising. IEEE Trans Image Process 29:5121–5135. https://doi.org/10.1109/TIP.2020.2980116
7. Shukla AK, Pandey RK, Yadav S, Pachori RB (2020) Generalized fractional filter-based algorithm for image denoising. Circuits Syst Signal Process 39:363–390. https://doi.org/10.1007/s00034-019-01186-y
8. Fang F, Li J, Yuan Y, Zeng T, Zhang G (2020) Multilevel edge features guided network for image denoising. Neural Netw Learn Syst IEEE Trans. https://doi.org/10.1109/TNNLS.2020.3016321
9. Li D, Chen H, Jin G, Jin Y, Zhu C, Chen E (2020) A multiscale dilated residual network for image denoising. Multimedia Tools Appl. https://doi.org/10.1007/s11042-020-09113-z
10. Pang ZF, Zhang HL, Luo S, Zeng T (2020) Image denoising based on the adaptive weighted TVp regularization. Signal Process 167:107325. https://doi.org/10.1016/j.sigpro.2019.107325
11. Zeng H, Xi X, Kong W, Cui S, Ning J (2020) Hyperspectral image denoising via combined non-local self-similarity and local low-rank regularization. IEEE Access 8:50190–50208. https://doi.org/10.1109/ACCESS.2020.2979809
12. Shukla AK, Pandey RK, Reddy PK (2020) Generalized fractional derivative based adaptive algorithm for image denoising. Multimedia Tools Appl. https://doi.org/10.1007/s11042-020-08641-y
13. Shin YH, Park MJ, Lee OY, Kim JO (2020) Deep orthogonal transform feature for image denoising. IEEE Access 8:66898–66909. https://doi.org/10.1109/ACCESS.2020.2986827
14. Elhoseny M, Shankar K (2019) Optimal bilateral filter and convolutional neural network based denoising method of medical image measurements. Measurement 143:125–135. https://doi.org/10.1109/ACCESS.2020.2986827
15. Kumar A, Ahmad MO, Swamy MNS (2019) Image denoising via overlapping group sparsity using orthogonal moments as similarity measure. ISA Trans 85:293–304. https://doi.org/10.1016/j.isatra.2018.10.030
16. Zha Z, Zhang X, Wang Q, Bai Y, Chen Y, Tang L, Liu X (2018) Group sparsity residual constraint for image denoising with external nonlocal self-similarity prior. Neurocomputing 275:2294–2306. https://doi.org/10.1016/j.neucom.2017.11.004
17. Fan L, Li X, Fan H, Zhang C (2019) An adaptive boosting procedure for low-rank based image denoising. Signal Process 164:110–124. https://doi.org/10.1016/j.sigpro.2019.06.004
18. Wang G, Liu Y, Xiong W, Li Y (2018) An improved non-local means filter for color image denoising. Optik 173:157–173. https://doi.org/10.1016/j.ijleo.2018.08.013

19. Li H, Suen CY (2016) A novel non-local means image denoising method based on grey theory. Pattern Recognit 49:237–248. https://doi.org/10.1016/j.patcog.2015.05.028
20. Chen G, Zhang P, Wu Y, Shen D, Yap PT (2016) Denoising magnetic resonance images using collaborative non-local means. Neurocomputing 177:215–227. https://doi.org/10.1016/j.neucom.2015.11.031
21. Wang X, Shen S, Shi G, Xu Y, Zhang P (2016) Iterative non-local means filter for salt and pepper noise removal. J Visual Commun Image Represent 38:440–450. https://doi.org/10.1016/j.jvcir.2016.03.024
22. Frosio I, Kautz J (2018) Statistical nearest neighbors for image denoising. IEEE Trans Image Process 28:723–738. https://doi.org/10.1109/TIP.2018.2869685
23. Rakhshanfar M, Amer MA (2019) Efficient cascading of multi-domain image Gaussian noise filters. J Real-Time Image Proc. https://doi.org/10.1007/s11554-019-00868-9
24. Hounsou N, Sanda Mahama AT, Gouton P, Thomas JB (2018) Comparative study of biorthogonal wavelets accuracy in demosaicing algorithm based on wavelet analysis of luminance component. Electronic Imaging 2018:362–371. https://doi.org/10.2352/ISSN.2470-1173.2018.16.COLOR-362
25. Wu H, Jia L, Meng Y, Liu X, Lan J (2018) A novel adaptive non-local means-based nonlinear fitting for visibility improving. Symmetry 10:741. https://doi.org/10.3390/sym10120741
26. Alelaiwi A, Abdul W, Dewan MS, Migdadi M, Muhammad G (2016) Steerable pyramid transform and local binary pattern based robust face recognition for e-health secured login. Comput Electr Eng 53:435–443. https://doi.org/10.1016/j.compeleceng.2016.01.008
27. Li L, Yu X, Jin Z, Zhao Z, Zhuang X, Liu Z (2020) FDnCNN-based image denoising for multi-labfel localization measurement. Measurement 152:107367
28. Zhang F, Fan H, Liu P, Li J (2020) Image denoising using hybrid singular value thresholding operators. IEEE Access 8:8157–8165. https://doi.org/10.1109/ACCESS.2020.2964683
29. Hore A, Ziou D (2010) Image quality metrics: PSNR vs. SSIM. In 2010 20th international conference on pattern recognition, IEEE, 2366-2369. https://doi.org/10.1109/ICPR.2010.579
30. Zhang L, Zhang L, Mou X, Zhang D (2011) FSIM: a feature similarity index for image quality assessment. IEEE Trans Image Process 20:2378–2386. https://doi.org/10.1109/tip.2011.2109730
31. Awad A (2019) Denoising images corrupted with impulse, Gaussian, or a mixture of impulse and Gaussian noise. Eng Sci Technol Int J 22:746–753. https://doi.org/10.1016/j.jestch.2019.01.012
32. Huang XL, Ma X, Hu F (2018) Machine learning and intelligent communications. Mobile Netw Appl 23(1):68–70
33. Huang XL, Tang X, Huan X, Wang P, Wu J (2018) Improved KMV-cast with BM3D denoising. Mobile Netw Appl 23(1):100–107

Publisher's Note Springer Nature remains neutral with regard to jurisdictional claims in published maps and institutional affiliations.